World Electric Vehicle Journal

MDPI

Article

Energy-Saving Impact and Optimized Control Scheme of Vertical Load on Distributed Electric Wheel Loader

Wenlong Shen [1,2], Yunwu Han [2], Xiaotao Fei [2,3] and Changying Ji [1,*]

[1] College of Engineering, Nanjing Agricultural University, Nanjing 210031, China; 1401003@jsei.edu.cn
[2] Department of Automobile Engineering, Jiangsu Vocational College of Electronics and Information, Huai'an 223003, China; gs59709@student.upm.edu.my (X.F.)
[3] Department of Mechanical & Manufacturing, Faculty of Engineering, Universiti Putra Malaysia, Serdang 43400, Malaysia
* Correspondence: chyji@njau.edu.cn

Abstract: During the operation of a wheel loader, the external load acting on the bucket undergoes many changes, resulting in significant changes in the load ratio on the front and rear axles. For this reason, controlling a standard wheel loader is not trivial. In addition, in the case of a distributed electric wheel loader (DEWL), the operating control algorithm is often complex and is, therefore, the subject of optimization studies. This study compared the electric power consumption across different vertical loads, speeds, and travel directions for single-front, single-rear, and dual-motor configurations, both during transporting and pre-shoveling operations. The analysis led to the development of control rules based on energy-saving objectives. Under the shoveling condition, it was observed that vertical loads can lead to an insufficient driving force and skidding, necessitating the proposal of a new optimized control scheme. The results revealed that the optimal solution for transporting is the single-motor drive control scheme without a mechanical connection between the front and rear motor. With the single-motor control scheme, comparing the preferred controlled motor with the unselected motor under different loads, the average electrical power savings for forward, backward, and circling were at least 3.51%, 3.12%, and 0.34%, respectively. Under the pre-shoveling condition, the optimal control scheme was identified as the single rear motor control scheme, effectively reducing electrical power consumption. In response to the issues encountered during the shoveling condition, an economical solution involving the modification of the front axle transmission ratio has been proposed, along with an optimized control scheme based on vertical load variations.

Keywords: distributed electric wheel loader; control scheme; vertical load; energy saving

Citation: Shen, W.; Han, Y.; Fei, X.; Ji, C. Energy-Saving Impact and Optimized Control Scheme of Vertical Load on Distributed Electric Wheel Loader. *World Electr. Veh. J.* **2024**, *15*, 141. https://doi.org/10.3390/wevj15040141

Academic Editor: Joeri Van Mierlo

Received: 11 March 2024
Revised: 27 March 2024
Accepted: 28 March 2024
Published: 30 March 2024

1. Introduction

As a piece of multi-functional heavy machinery equipment, the loader can be used in diverse operational environments by utilizing various attachments, such as a bucket, fork, clamp, and crushing hammer [1]. The primary attachment for loaders is the bucket, which is utilized for excavating, transporting, and loading materials such as soil, sand, and crushed stones. It is extensively implemented in construction sites, mines, and agriculture applications. The fork is employed for handling and stacking materials, which is suitable for warehouse, logistics, and freight scenarios. The clamp is utilized for gripping, grabbing, and transporting irregularly shaped objects, playing a crucial role in wood processing, construction, and manufacturing industries [2,3]. Electric loaders have some significant advantages in engineering over conventional fuel-driven loaders [4–7]:

- Environmental protection and sustainability. Electric loaders utilize electricity, reducing dependence on fossil fuels and thereby decreasing greenhouse gas emissions and other environmental pollution. In countries and regions where strict environmental regulations are enforced or in environmentally friendly production environments, electric loaders emerge as an ideal choice, aligning with the principles of sustainable development.

- Reduced noise and vibration. Electric loaders typically produce less noise and vibration than conventional internal combustion engines. This characteristic contributes to an improved working environment and reduces potential health impacts on operators.
- Indoor operation. Due to the lack of exhaust emissions and low noise level of electric loaders, they are better suited to operations in indoor environments or places where indoor control is necessary, such as greenhouses, warehouses, and similar settings.
- Lower operating costs. Electric loaders typically have lower operating costs because electricity is cheaper and more stable than fuel. In addition, electric machines usually require less maintenance, resulting in reduced upkeep expenses. This represents an economically viable option for businesses, enhancing cost-effectiveness in production.
- Improved energy efficiency. Electric loaders typically demonstrate superior energy efficiency. They can improve overall energy efficiency by recovering braking energy, intelligent battery management systems, and other technologies that reduce energy waste.
- Flexibility and adjustability. Electric loaders typically have better adjustability, allowing them to precisely control speed and power output as needed. This flexibility makes them more suitable for different tasks, thus increasing efficiency.

In 2023, electric loader sales in China surged to 3595 units, comprising 6.36% of total loader sales, marking a remarkable year-on-year increase of over 200% compared to 2022. During September, October, and November, the monthly market share of electric loaders consistently exceeded 10%, registering figures of 10.3%, 14%, and 10.4%, respectively [8]. With the rapid advancement in electric vehicle technology, the advent of new technologies has significantly decreased the costs associated with batteries, motors, and electronic control assemblies. Electric wheel loaders (EWLs) boast advantages such as a high torque at low speeds, minimal working noise, low vibration, and zero exhaust emissions, making them highly suitable for industrial and agricultural applications. Moreover, compared to traditional wheel loaders with internal combustion engines, EWLs offer the additional benefits of reduced maintenance and lower operating costs, promising a favorable market outlook. Presently, the Chinese market features a total of 13 companies offering 40 models of electric wheel loaders, as outlined in Table 1 [9]. The majority of these loaders operate on a dual-motor system, with one motor dedicated to the front and rear axles through the gearbox for driving purposes, while another motor is responsible for the hydraulic system. These loaders are commonly referred to as centralized electric wheel loaders (CEWLs). In contrast, XCMG's electric wheel loaders, excluding the XC918-EV, utilize three motors for power. Each front and rear axle has its dedicated motor for driving, and a separate motor handles the hydraulic system. When the front and rear axle motors operate independently, this loader configuration is termed a distributed electric wheel loader (DEWL). The notable advantage of DEWLs lies in the absence of a gearbox, leading to reduced maintenance costs, faster response in overall machine movement, lower energy loss, and more energy-efficient travel. But in fact, to ensure sufficient power during shoveling, the front and rear motors are mechanically interconnected through the drive shaft, as depicted in Figure 1. Consequently, DEWLs effectively revert to CEWLs. According to Yang, Z. et al., CEWLs generate parasitic power due to steering radius differences, tire radius differences, ground conditions, and actual working conditions [10,11]. When continuously driving for one hundred kilometers under a 5-ton standard block load with parasitic power generation, the power consumption loss accounts for nearly one-fifth of the battery capacity, highlighting the considerable negative impact of parasitic power on loaders. Therefore, it is of great practical significance to study the DEWL control method.

Figure 1. Mechanical connection of front and rear driving motors of XCMG electric wheel loader.

Table 1. Main parameters of EWL for sale in the Chinese market.

Manufacturer	Product Model	Rated Load Capacity (kg)	Operating Weight (kg)	Bucket Capacity (m^3)	Max. Breakout Force (kN)	Travel Rated Power (kW)
SEM	SEM658F	5500	17,600	2.6~5.0	178	/
SDLG	L968HEV	6500	22,300	3.0~6.0	180	125
	L956HEV	5500	19,000	2.7~4.5	170	125
LiuGong	820TE	2000	6400	1.2~1.5	50	60
	856HE	5500	18,035	2.7~5.6	175	180
	856HE MAX	5800	19,800	2.7~5.6	185	180
	862HE	6500	20,100	2.7~5.6	190	190
	870HE	7500	24,206	3.0~7.0	220	210
	870HE MAX	7500	24,206	3.0~7.0	220	210
XGMA	XG958EV	5500	18,500	2.2~4.5	160	150
ShanTui	LE39-X3	3000	11,500	1.5~3.0	105	52
	LE59-X2	5500	18,000	2.6~5.0	185	150
	LE60-X3	5800	18,500	4.0~5.0	185	100
	LE70-X3	6500	22,300	4.0~5.5	205	120
XCMG	XC918-EV	1800	6700	0.5~1.5	62	64
	XC958-EV	5800	18,700	2.0~5.0	177	180
	XC968-EV	6000	19,100	2.5~5.5	174	180
	XC975-EV	7000	23,160	3.5~5.0	195	180
	XC9350-EV	35,000	150,000	18	961	970
SANY	SW956E	5800	19,000	2.7~5.0	182	255
	SW966E	6800	23,200	2.7~6.0	210	225
LOVOL	FL960EV	5800	19,400	2.7~5.0	165	125
	FL966EV	6500	22,300	2.7~6.0	170	125
	FL968K-E	6500	23,660	2.7~6.0	/	/
JINGONG	JGM857E	5500	18,500	2.7~5.0	170	100
CHANGLIN	950E	5000	20,400	2.2~4.5	174	189
	955Ev	5000	18,000	2.2~4.5	174	189
LonKing	ZL50NC-E	5000	17,300	2.7~5.0	180	/
	LG856H-E	5500	18,100	2.7~5.0	180	/
	LG866H-E	6500	21,900	3.5~5.6	210	/

Table 1. *Cont.*

Manufacturer	Product Model	Rated Load Capacity (kg)	Operating Weight (kg)	Bucket Capacity (m^3)	Max. Breakout Force (kN)	Travel Rated Power (kW)
ENSIGN	YX656EV-S	5500	18,460	2.4~4.5	165	120
	YX656EV	5500	19,260	2.4~4.5	167	120
	YX656EV-GT	5500	19,260	2.5~5.6	165	120
	YX660EV-GT	5800	19,100	2.4~4.5	190	120
BRETON	BRT936EV	3000	10,700	1.7~2.5	95	120
	BRT958EV	5500	18,200	2.7~4.2	176	220
	BRT966EV	6600	23,600	3.6~5.6	210	340

Jiang, T. et al. analyzed the drive power consumption characteristics of electric vehicles with independent front and rear axle drives. They proposed a method for calculating the torque distribution coefficient, utilizing the total power loss of the front and rear motors as the target function [12]. Yang, Z. et al. developed a longitudinal dynamics model for a front/rear axle electric wheel loader (FREWL). They formulated objective functions aimed at minimizing the weighted sum of tire workload variance and mean, while maximizing total motor efficiency. Four nonlinear constraint optimization algorithms, namely the quasi-Newton Lagrangian multiplier method, sequential quadratic programming, adaptive genetic algorithms, and particle swarm optimization with random weighting and natural selection, were employed to solve the objective function. The simulation results showed that compared to no-control FREWLs, controlled FREWLs exhibited a better utilization of adhesion ability and reduced slipping. The energy efficiency in equipment transfer conditions for the FREWL increased by 13~29% [13]. Fei, X. et al. examined the energy consumption efficiency of DEWLs across three propulsion modes: front motor drive, rear motor drive, and dual-motor drive. Their analysis considered the variation in drive force demand resulting from bucket landing [14]. Cai, S. et al. proposed a comprehensive automatic shifting control strategy that balances both power and economy, achieving ideal power performance and energy-saving effects [15]. K. Uebel et al. argued that conventional design optimization methods for road vehicles are unsuitable for loaders operating repetitively over short periods with high transient power output. They suggested that a rule-based simple energy management strategy is sufficient to find the optimal hardware design [16]. A simulation model for an integrated wheel loader was proposed to enhance performance and energy flow. This model predicted and evaluated optimization paths, energy flow, and loss analysis during V-type operation, among other work performances. Also, the model could study the optimal working modes and energy flow for various working cycles of wheeled loaders [17]. Gao et al. employed the singular value decomposition unscented Kalman filter to estimate the shovel load. Based on the estimated shovel load, they calculated the vertical tire force. The tire load ratio was used to establish optimization goals, with drive anti-slip set as a boundary condition. The optimized strategy showed fewer instances of slipping, with a higher traction force and efficiency compared to non-control strategies [18]. Sondkar, P. proposed a longitudinal vehicle dynamics model for a four-wheel drive system to understand the impact of various key factors on the torque distribution between the front and rear axles [19]. Yuan et al. suggested that in the low torque range, front and rear-wheel-drive electric vehicles should operate only one motor to provide the required total torque. They designed an online optimized torque distribution algorithm to determine whether the second motor should be disengaged from the clutch in the low torque range. Adopting the proposed optimization scheme led to an improvement of 4% in the efficiency of the drive train over the New European Driving Cycle (NEDC) [20]. To enhance the economy of a multi-axle electric vehicle, an optimal drive distribution control strategy was proposed. This strategy prioritized the optimal efficiency of the electric drive system by selecting specific drive axles based on the dynamic distribution of the axle loads, thereby maximizing ground adhesion utilization. The findings revealed that the optimal drive torque distribution control strategy enhances efficiency by 9.18% compared to the average drive torque distribution control strategy [21]. For multi-axle distributed vehicles, stability weight adjustment coefficients were introduced in the torque distribution strategy to achieve the multi-objective optimization of the tire load rate and energy efficiency. The simulation analysis results showed that the torque distribution can be reduced by approximately 8% in energy consumption compared to the inter-axle torque allocation strategy [22]. To reduce energy consumption during the steering condition for multi-axle electric vehicles, the deep deterministic policy gradient (DDPG) algorithm was proposed, resulting in a decrease of approximately 5% in the maximum SOC degradation rate of the vehicle [23]. To address the issues of low fuel efficiency and ineffective switching control in distributed-wheel-side four-wheel-drive electric buses, researchers proposed a golden section search algorithm. This algorithm aimed to determine the optimal front–rear axle motor torque distribution coefficient, denoted as K, by considering the efficiency characteristics of the front and rear axle drive motors. Compared to the equal distribution to all four wheels, the new algorithm improved efficiency by 4.35% and 3.83% under two different steering conditions [24]. A load torque-based control strategy (LTCS) was designed using the particle swarm optimization algorithm (PSO), and a working point corresponding to the optimal energy conversion efficiency was selected to control the motor's operating state. Tractor traction experiments were simulated, and the results demonstrated that the LTCS could efficiently utilize electric energy in tractors while maintaining agricultural applicability under field conditions [25]. A combined control method based on the active torque distribution, considering the driving speed and slip, was proposed and applied to an independently driven electric tractor. The results showed that compared to the torque average distribution mode, the new method reduced the slip of the tractor by 14.1%, decreased the motor energy consumption by 6.8%, and improved the traction efficiency by 6.8% [26].

The aforementioned research mainly focuses on the energy-saving scheme for the DEWL, emphasizing torque distribution optimization to reduce mechanical power while giving less consideration to the impact on system power consumption. The operating conditions of electric passenger cars, commercial vehicles, tractors, and loaders are not consistent, especially when heavy-duty operations are performed by loaders. The significant vertical loads on the front and rear axles can have a considerable impact on vehicle performance. Thus, it may not completely address the relevant issues of DEWLs.

2. Methodology

2.1. Experimental Subject

The DEWL, featuring a battery voltage of 580 V, serves as the chosen test subject in this research, as depicted in Figure 2. The DEWL is a modification of a ZL50 loader, which is a wheel loader with a rated load capacity of 50 kN. The DEWL is equipped with two electric motors for driving and one electric motor for the hydraulic system. Both driving motors share identical specifications in terms of rated power and torque. Additionally, these motors can independently or collaboratively output power, and they can also be mechanically linked by a shaft for joint power output. The energy consumption of the DEWL during the running condition is influenced by numerous parameters. Table 2 provides detailed information on the specific parameters of the DEWL.

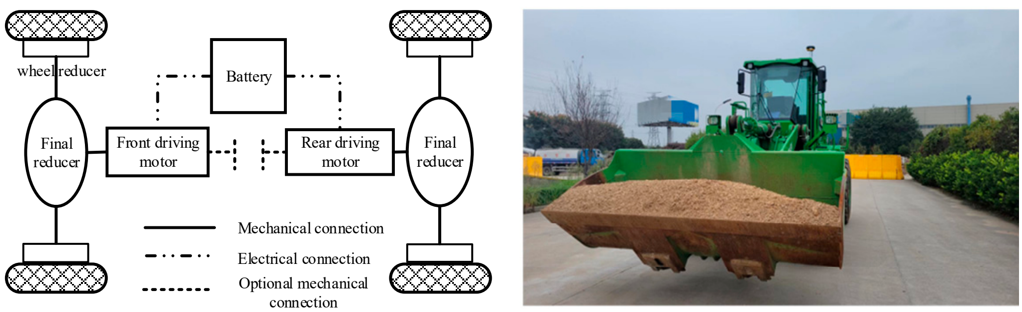

Figure 2. Schematic diagram of the DEWL mechanical and electrical connection.

Table 2. Parameters of distributed electric wheel loader.

Parameters	Value	Unit
Rated load	5.3	t
Volume of bucket	3.2	m^3
Mass of the loader	17 ± 0.5	t
Wheelbase	3300	mm
Maximum shoveling force	>175	kN
Maximum traction force	>165	kN
Type of tires	23.5-25-16PR	/
Tire diameter	1610	mm
Overall dimensions (L×W×H)	$8650 \times 3000 \times 3520$	mm
Resultant gear ratio	22.85	/

2.2. Hardware and Software for Test

The driving motor is governed by the Vehicle Control Unit (VCU). Therefore, to facilitate vehicle control, the development of VCU software is imperative. The VCU's composition, illustrated in Figure 3, is categorized into the controller housing, hardware circuit, underlying software, and application layer software [27]. As shown in Figure 4, all hardware components communicate through the Controller Area Network (CAN) bus, operating at a baud rate of 250 kb/s. CANH and CANL are the names of two signal lines used for transmitting high- and low-level signals on the CAN bus, respectively. The software required for the vehicle experiments is written in MATLAB/Simulink.

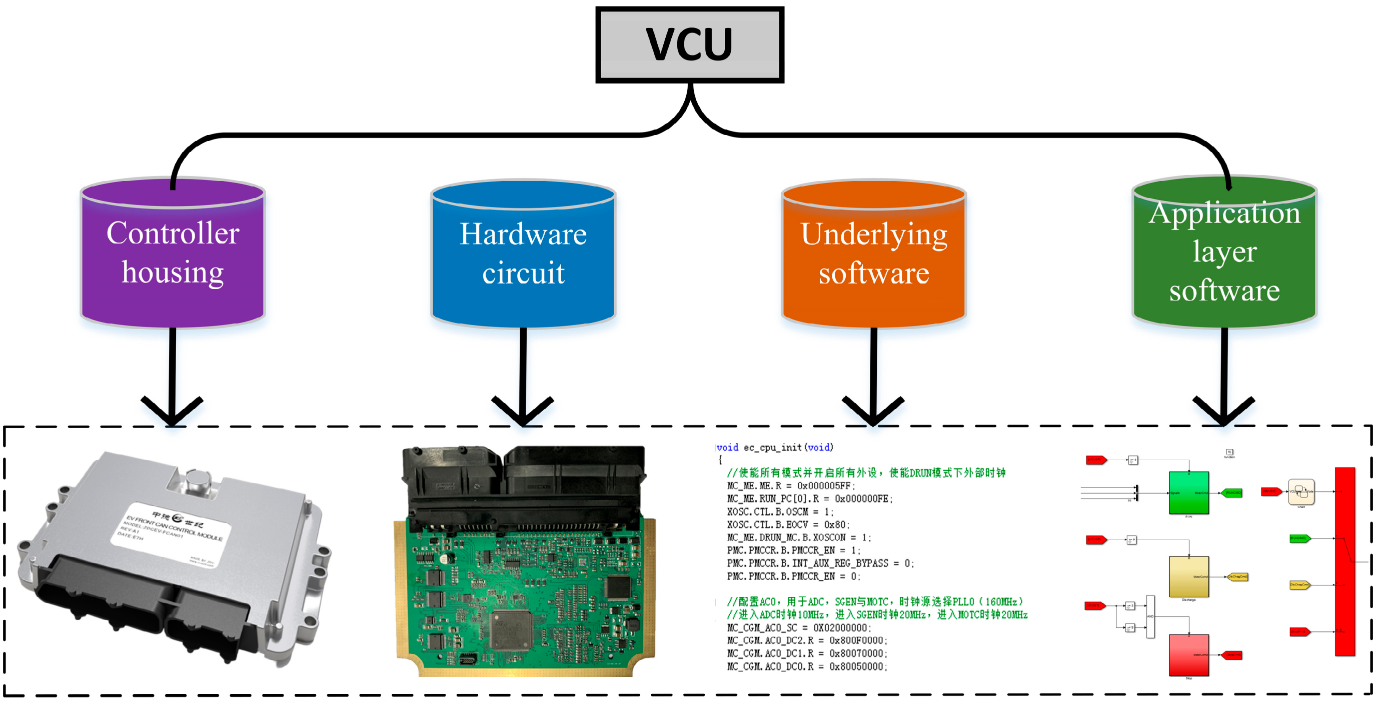

Figure 3. Vehicle Control Unit Components.

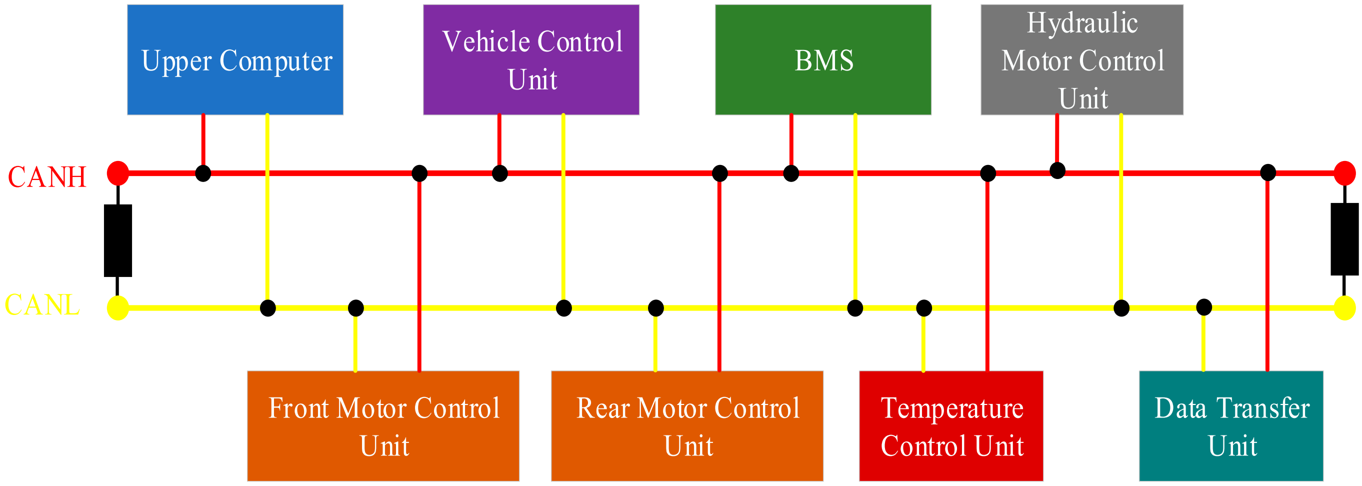

Figure 4. The network topology of the hardware system.

2.3. The System Efficiency MAP of Motor

Through the motor experiment platform, we tested the characteristics of the drive motor at different torques, covering speeds of 500 rpm, 1000 rpm, 1500 rpm, 2000 rpm, 2500 rpm, and 3000 rpm. During these tests, we recorded the motor's current, voltage, and electric power. Subsequently, we calculated both the motor efficiency and controller efficiency. Finally, a map of the motor system efficiency was created, which is crucial for the development and optimization of control algorithms [28]. As depicted in Figure 5, the upper half is the motor discharge efficiency, while the lower half is the motor power generation efficiency. During the test, the DEWL operated at a low speed and the motor speed was maintained below 1000 rpm. It was observed that the motor system efficiency of the DEWL increased with the torque increment during these operations.

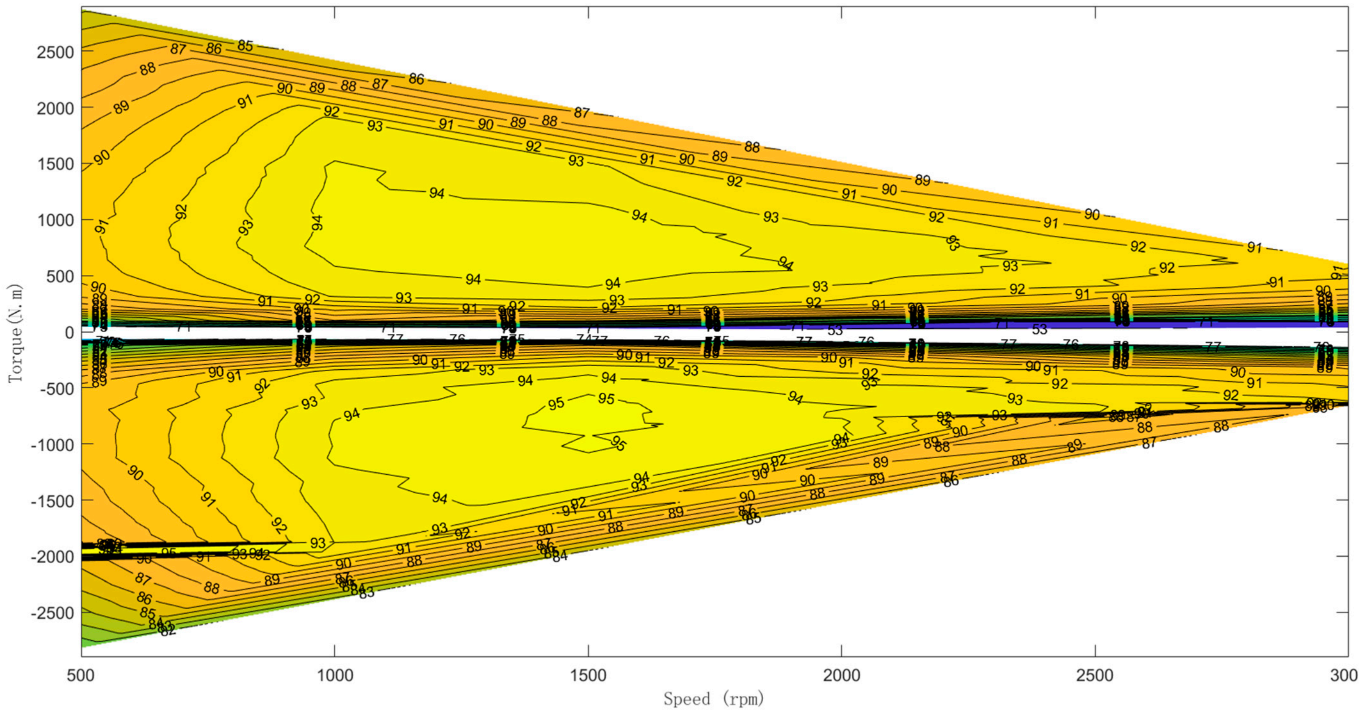

Figure 5. Driving motor system efficiency map.

2.4. Experiment Design

The transportation and pre-shoveling condition experiments involved the DEWL traveling on a horizontal concrete road to ensure the stability of experimental data. For the shoveling condition experiments, the DEWL operated on authentic off-road surfaces, engaging in real material handling tasks.

2.4.1. Transporting Condition

Under the transporting condition, the motor connection mode was categorized into 2 modes: mechanical and non-mechanical connection. According to the transporting track, it was divided into 3 modes: straight forward, straight backward and circling (turning angle is 32° measured by Vert-X 88 series angle sensor from Contelec). Additionally, based on the different motor drive methods, it was segmented into 3 modes: front motor drive, rear motor drive, and dual-motor drive. Therefore, there were a total of 18 cases, with Table 3 displaying 9 of these cases.

Table 3. Test for 9 cases of EWL under transporting condition.

Status	Description
FF	The front motor independently drives forward in straight line.
FB	The front motor independently drives backward in straight line.
FC	The front motor independently drives positive circling.
RF	The rear motor independently drives forward
RB	The rear motor independently drives backward.
RC	The rear motor independently drives positive circling.
DF	Dual-motor drive forward in straight line.
DB	Dual-motor drive backward in straight line.
DC	Dual-motor drive positive circling.

The front and rear drive motors implemented speed control, selecting target speeds of 200, 400, 600, 800, and 1000 rpm, and an experienced loader driver shoveled sand–gravel material loads. The bucket loads weighed 0 tons (no load), 2.15 tons (1/3 load), 3.35 tons (2/3 load), and 4.54 tons (full load), which were actually measured by the weighbridge. During the transporting condition, the bottom of the bucket was positioned 60 cm from the ground. The experimental data included the speed, torque, current, and voltage of both the front and rear motors, as well as the bus voltage and current, as shown in Figure 6. As the loader reached the target speed from the static state, the speed exhibited a roughly linear rise. In the curves, "FS" indicates the front motor speed in rpm, "RS" indicates the rear motor speed in rpm, "FT" indicates the front motor torque in N·m, "RT" indicates the rear motor torque in N·m, "FI" indicates the front motor current in amps, "RI" indicates the rear motor current in amps, "FU" indicates the front motor voltage in volts, "RU" indicates the rear motor voltage in volts, "I" indicates the bus-bar current in amps, and "U" indicates the bus-bar voltage in volts. The two motor output shafts are arranged in the opposite direction, the speed and torque of the front motor are positive, while the speed and torque of the rear motor are negative when the DEWL is moving forward.

When the motor feedback speed reached the target speed, there was a significant fluctuation in the feedback torque. To prevent the influence of data during this fluctuation stage on the accuracy of the experimental results, the data within this stage were excluded by setting a reasonable threshold range. Subsequent analysis focused on the data obtained during the steady-state stage.

Since the recorded data are discrete and not directly integrable, the average method is employed for approximations, as illustrated in Equations (1) and (2). Equation (1) is the calculation of mechanical work; Equation (2) is the calculation of electrical work. The average system efficiency of the motor can be calculated using Equation (3).

$$W_{out} = \int_j^k \frac{T_i \cdot n_i}{9549} dt \approx (t_k - t_j) \cdot \overline{P_T} = (t_k - t_j) \cdot \frac{\sum_j^k T_i \cdot n_i}{9549(k - j + 1)} \quad (1)$$

$$W_{\text{in}} = \int_j^k U_i \cdot I_i dt \approx (t_k - t_j) \cdot \overline{P_{UI}} = (t_k - t_j) \cdot \frac{\sum_j^k U_i \cdot I_i}{k - j + 1} \quad (2)$$

$$\overline{\eta_{sys}} = \frac{\overline{P_{out}}}{\overline{P_{in}}} = \frac{\overline{P_T}}{\overline{P_{UI}}} \times 100\% \quad (3)$$

W_{out} represents output work, i.e., mechanical work, while W_{in} represents input work, i.e., electrical work. t_j represents the starting time, and t_k represents the ending time. $\overline{\eta_{sys}}$ means the average system efficiency of the driving motor. $\overline{P_T}$ and $\overline{P_{UI}}$ represent the average mechanical power and electrical power of the driving motor.

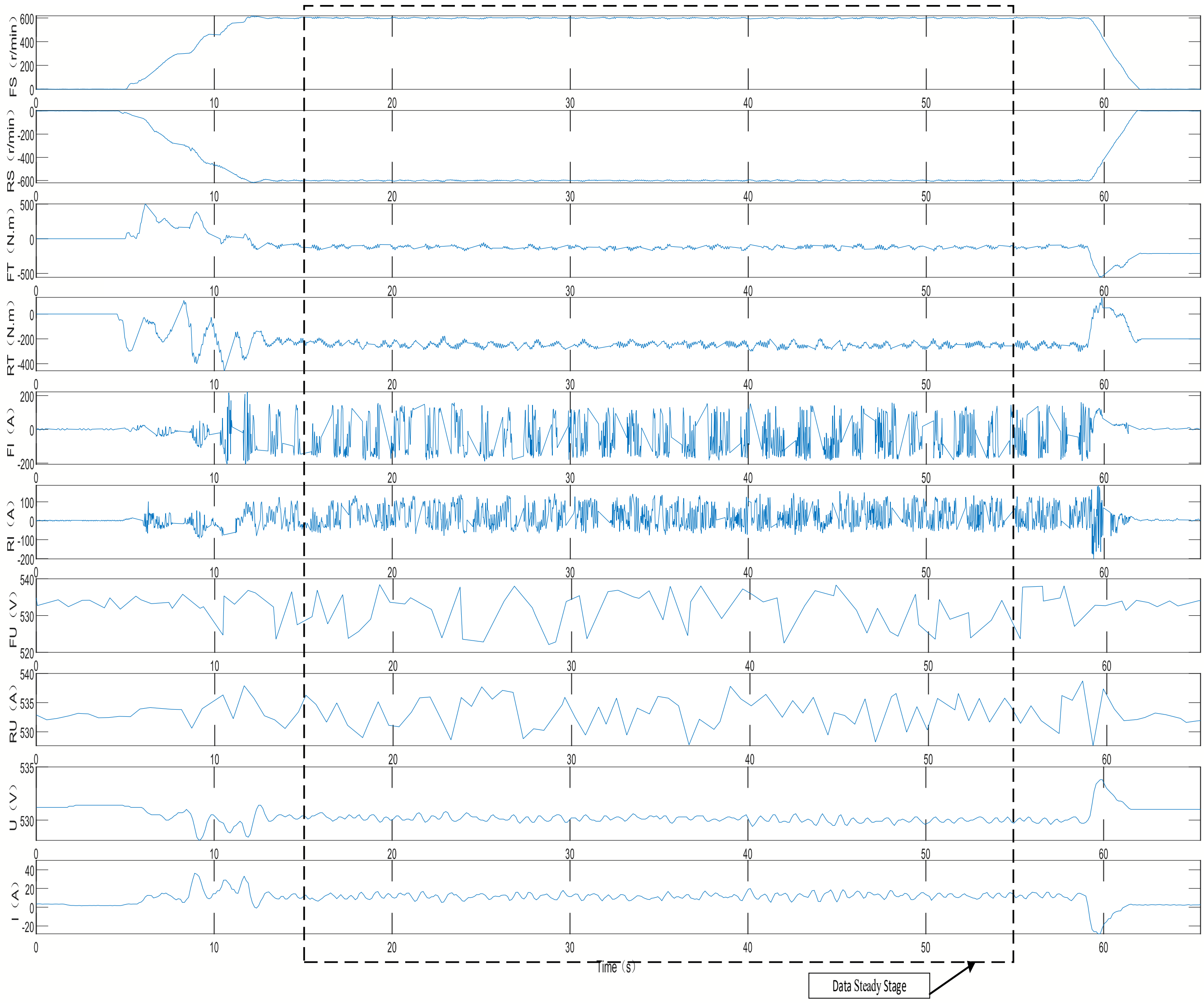

Figure 6. Experimental data at steady state of driving motor.

Meanwhile, changes in the front and rear wheel tire radius, as well as alterations in the center of gravity, were measured under static conditions. The tire radius was measured using a laser range finder, gauging the distance from the highest point of the tire to the ground. The DEWL center of gravity measurements were conducted using the floor scale to measure the front and rear axle loads separately.

2.4.2. Pre-Shoveling Condition

Under the pre-shoveling condition, the height and angle of the bucket was adjusted before digging the material to simulate real loader scenarios [14]. The test simulated four states: where the front wheels were slightly lifted, lifted more, slightly off the ground, and lifted more off the ground. As above, it was divided into three modes: front motor drive, rear motor drive, and dual-motor drive, resulting in 12 cases. However, in cases F3 and F4, the driving wheels were the front wheels; at this time, the front wheels left the ground without valid data, so they were eliminated. And similarly, in case D4, the driving wheels were driven by both the front and rear wheels together, and there was no valid data for the front wheels, which was also eliminated, as shown in Table 4. The target speed for the motor was set at 600 rpm.

Table 4. Test for 9 cases of EWL under pre-shoveling condition.

Status	Driving Motor	Bucket Tooth Tip in Relation to the Ground	Vertical Force
F1	Front	Parallel	Low
F2	Front	Parallel	Large
R1	Rear	Parallel	Low
R2	Rear	Parallel	Large
R3	Rear	Small angle contact	Larger
R4	Rear	Large angle contact	Larger
D1	Front and rear	Parallel	Low
D2	Front and rear	Parallel	Large
D3	Front and rear	Small angle contact	Larger

According to the motor control protocol and vehicle control protocol provided by the manufacturer, the collected data are interpreted as follows: When the loader is driven forward by the dual-motor system, the front motor speed and torque are positive; the rear motor speed and torque are negative. Conversely, when the loader is reversed using dual-motor drive, the conditions are reversed. Regardless of any situation, the current is positive when the motors are discharging; the current is negative when the motors are generating. Under the pre-shoveling condition, the method is basically the same as in the transporting condition. The test site is located on the cement pavement in the factory area. Each test is conducted three times, covering a round trip of 300 m.

2.4.3. Shoveling Condition

The maximum breakout force of the DEWL depends on the collaborative work of all motors, currently employing a control strategy that evenly distributes the desired torque between the front and rear motors. During the actual shoveling process, the front axle bears an extremely high vertical load [29,30]. This concentrated load on the front axle reduces the adhesion of the rear wheels, potentially leading to tire slippage and inadequate total driving force for the DEWL. Hence, optimizing the motor control strategy to prevent slippage and ensure adequate driving force is paramount in DEWL shoveling conditions.

3. Results

Table 5 presents the data of the front and rear wheel heights and axle load ratios under different loads, with the bucket height above the ground set at 60 cm. The DEWL is equipped with four 23.5-25-16 PR tires, and the standard tire outer diameter is 1615 mm. With the increasing load, the center of gravity gradually shifts forward, leading to a gradual decrease in the height of the front wheels and an increase in the height of the rear wheels.

Table 5. Front and rear wheel heights and axle load ratios under different loads.

Load	No Load	1/3 Load	2/3 Load	Full Load
Front Wheel Height (mm)	1511	1469	1444	1416
Rear Wheel Height (mm)	1494	1507	1517.6	1530
Front Axle Load Ratio	0.4593	0.5761	0.64	0.7004
Rear Axle Load Ratio	0.5407	0.4239	0.36	0.2996

3.1. Results of Transporting Condition

Tables A1–A8 in Appendix A present the data under the transporting condition, while Tables A9 and A10 in Appendix A display the data under the pre-shoveling condition.

Tables A1–A3 contain data for the transporting condition under three different loads and five target speeds. The front and rear motor of the loader were connected by coupling and a transmission shaft. As shown in Table A1, under one-third of a load, in most cases, when moving forward, the electrical power required for rear motor drive was approximately 0.9~14% lower than that required for front motor drive. When moving backward, the electrical power required for front motor drive was about 1.2~19.6% lower than that for the rear motor. But at 600 rpm, the pattern was reversed. When circling, the front and rear motors required approximately the same amount of electrical power. As shown in Table A2, under two-thirds of a load, when moving forward, the rear motor was more energy-saving than the front motor at 200 and 400 rpm, and the front motor was more energy-saving than the rear motor at 600, 800, and 1000 rpm. When moving backward, the electrical power required for front motor drive was about 18.4~30.5% lower than that for the rear motor. When circling, the electrical power required for the rear motor was 8.7–14.1% than that for the front motor. As shown in Table A3, under a full load, at 200 rpm, the rear motor saved energy when moving forward, and the front motor saved energy when moving backwards and circling. At 400 rpm, the difference was not significant. At 600 and 800 rpm, the energy-saving pattern was the same, with both being more energy-saving for the rear motor.

Table A4 represents data for the transporting condition with dual-motor drive, including torque, mechanical power, electrical power, and motor system efficiency, each with two columns. The first column corresponds to the front motor, while the second column represents the rear motor. In speed mode, to maintain consistent speed, one motor drives forward while the other brakes forward. In both statuses, the rear motor is driven and the front motor is braked. For the same load, speed, and direction of driving, dual-motor drive requires much more electrical power than single-motor drive.

Tables A5–A8 contain data for transporting conditions under four different loads and five target speeds. The front and rear motor of the loader were independent and had no mechanical connection. As shown in Table A5, under no load, whether moving forward, backward, or circling, front motor drive required more power than rear motor drive. Using the same motor, the torque and power required for circling were the largest, followed by backward driving, while forward driving was the most economical. With the increase in speed, the efficiency of the motor system was improved. As shown in Table A6, under one-third of a load, when moving forward, the electrical power required for rear motor drive was approximately 6~25% lower than that required for front motor drive. When moving backward, the electrical power required for front motor drive was about 4~26% lower than that required for rear motor drive. When circling, the front and rear motors required approximately the same amount of electrical power. As shown in Table A7, under two-thirds of a load, whether forward or backward, the electric power required by front motor drive was less than that required by the rear motor. Specifically, during forward driving at a target speed of 1000 rpm, front motor drive required 70% less electrical power than rear motor drive. When circling, the front and rear motors required approximately the same amount of electrical power. As shown in Table A8, under a full load, whether moving forward or backward, the electric power required for front motor drive was less than that required for rear motor drive.

3.2. Results of Pre-Shoveling Condition

As shown in Table A9, when the DEWL was driven using the front motor, the maximum average motor system efficiency was 43.73% in driving forward and 45.12% in driving backward. When the DEWL was driven using the rear motor, the maximum average motor system efficiency was 64.96% in driving forward and 68.17% in driving backward.

Table A10 includes torque, mechanical power, electrical power, and motor system efficiency, each with two columns of data. The first column represents the front motor, while the second column represents the rear motor. The torque and electric power required for dual-motor drive were significantly higher than those required by single-motor drive.

3.3. Results of Shoveling Condition

As shown in the Figure 7, the arrows indicate rear wheel slippage observed during the two dual-motor drive shoveling condition. It was observed that the torque output of the front motor approached its rated torque, while the rear motor idled at a high speed relative to the front motor. In extreme situations, it even appeared that the rear wheel lifted up with the front axle as the fulcrum, as shown in the Figure 8. The conventional response is to rigidly connect the two motors by means of a drive shaft to ensure that the shovel digging force is sufficient. This is why the loader manufacturer uses a driveshaft-connected dual-motor instead of the more efficient independently controlled motor solutions.

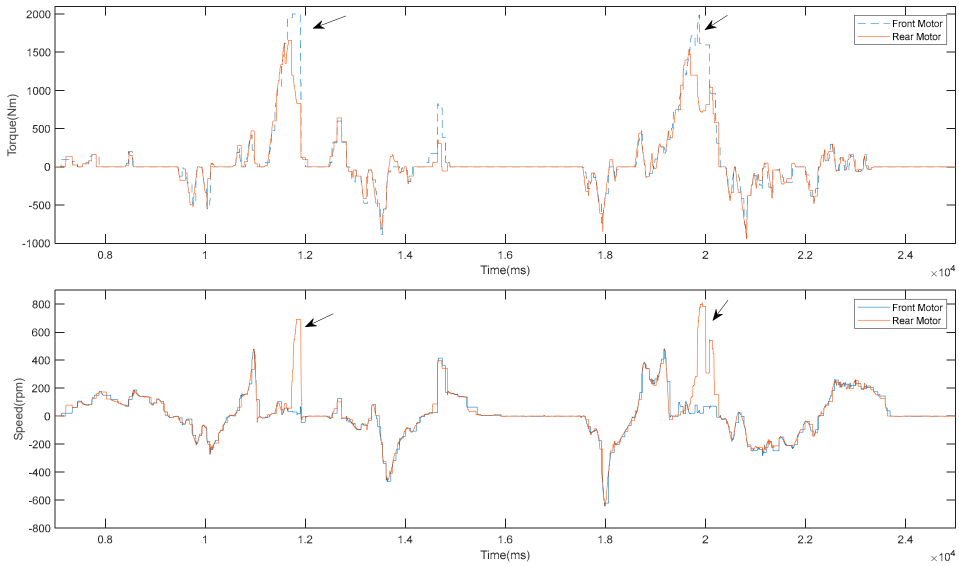

Figure 7. Dual-motor average torque distribution under shoveling condition.

Figure 8. The extreme situation of DEWL under shoveling condition.

4. Discussion

4.1. Control Scheme of Energy-Saving for DEWL under Transporting Condition

Currently, the torque distribution strategy for EWLs, particularly those with mechanically connected front and rear drive motors, typically involves evenly distributing the desired torque to both motors. Analyzing the motor system efficiency MAP diagram (Figure 5) reveals that, compared to single-motor drive, the mechanically connected dual-motor setup results in smaller averaged drive torque per motor. Consequently, this leads to lower motor efficiency and increased energy consumption. Additionally, the difference in wheel radius between the front and rear wheels introduces parasitic power through mechanical connections, further exacerbating energy consumption issues, as previously mentioned. Therefore, the mechanically connected dual-motor solution may not be conducive to meeting energy-saving requirements.

Tables A1–A3, when compared to Tables A6–A8, indicate that motors without mechanical connections generally require less mechanical and electrical power than motors with mechanical connections, especially when traveling in a straight line. Based on the results of Equation (4) illustrated Figure 9, the X-axis coordinates are labeled in accordance with Table 3. For instance, considering "FF200" as an example, "FF" denotes the state, indicating the front motor drives forward, while the number "200" signifies the motor speed of 200 rpm. Sometimes, the difference between the average speed of the driving motors and the target speed is large, but the energy saving effect is not obvious. Because the loader is affected by both the load and speed, this results in a bumpy ride and the phenomenon of slippage. However, mechanical connection solutions are found to be inferior to non-mechanical connection solutions in EWLs.

$$\lambda = \frac{\overline{P_{UI}}_{(with\ mechanical\ connection)} - \overline{P_{UI}}_{(without\ mechanical\ connection)}}{\overline{P_{UI}}_{(with\ mechanical\ connection)}} \tag{4}$$

$$\overline{\lambda} = \frac{\sum_i \frac{\overline{P_{UI}}_{(with\ mechanical\ connection)} - \overline{P_{UI}}_{(without\ mechanical\ connection)}}{\overline{P_{UI}}_{(with\ mechanical\ connection)}}}{i} \tag{5}$$

λ is the percentage of average electrical power savings, $\overline{P_{UI}}_{(with\ mechanical\ connection)}$ is the average electrical power of the motor when the front and rear axles are mechanically connected, $\overline{P_{UI}}_{(without\ mechanical\ connection)}$ is the average electrical power of the motor when the front and rear axles are not mechanically connected. $\overline{\lambda}$ is the average percentage of electrical power savings.

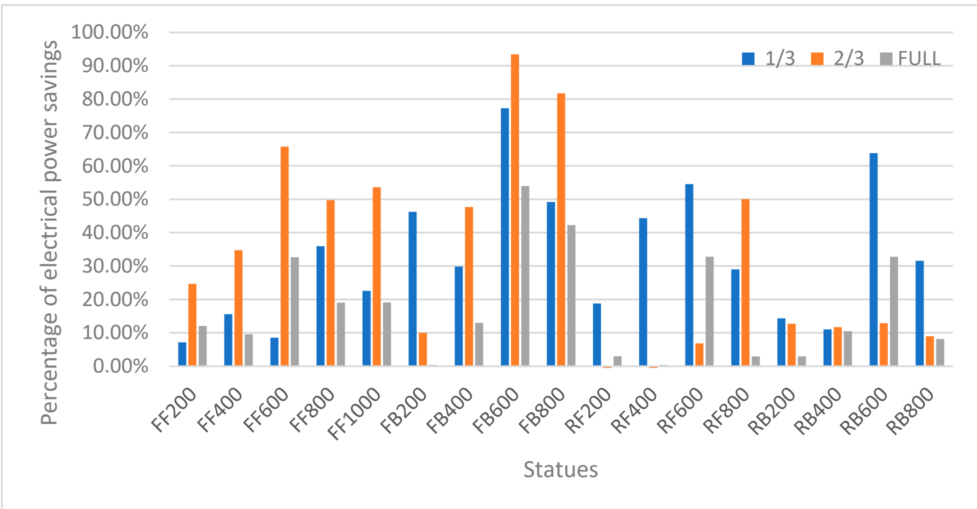

Figure 9. The percentage of electrical power savings with front and rear motor without mechanical connection.

Tables A4 and A5 reveal that under no load, a single-motor drive required less torque, mechanical power, and electrical power than dual-motor drive in the same situation. Compared to dual-motor drive, single front motor drive exhibited reductions of 30.25% in average torque, 30.51% in average mechanical power, and 38.10% in average electrical power during forward motion. Similarly, during backward motion, single front motor drive demonstrated reductions of 29.91% in average torque, 29.50% in average mechanical power, and 40.95% in average electrical power. In contrast, single rear motor drive, when compared to dual-motor drive, showed a decrease of 29.22% in average torque, 29.39% in average mechanical power, and 39.58% in average electrical power during forward motion. During backward motion, the single rear motor drive displayed reductions of 28.44% in average torque, 28.16% in average mechanical power, and 29.03% in average electrical power. Figure 10 presents the degree of electrical power savings with single-motor drive compared to dual-motor drive under various conditions with no load. It indicates that for the DEWL, the dual-motor drive is not as energy-efficient as the single-motor drive solution.

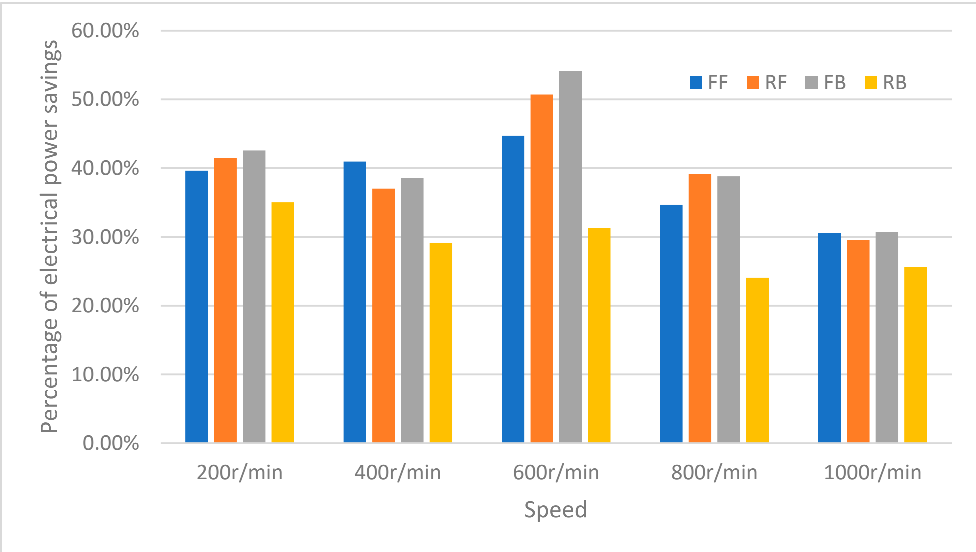

Figure 10. The percentage of electrical power savings with single-motor drive compared to dual-motor drive for transporting under no load conditions.

Tables A5–A8 show that the torque, mechanical power, and electrical power required by the DEWL increased with the raised load under the same statuses, following a consistent trend. However, under the same load, speed, and forward direction, the EWL's front and rear motor exhibited different torque and power requirements. The experimental data indicated minimal difference in mechanical power but significant disparity in electrical power. Traditionally, energy-saving perspectives have primarily focused on optimal torque distribution, often neglecting system efficiency. This paper explores energy-saving control schemes for the DEWL through a comparative analysis of system efficiency.

The data from Table A5 revealed that under no load, the rear motor drive consumed less power and had higher system efficiency when moving forward and backward. This is due to the larger rear axle load, smaller rear wheel radius, and the resulting need for larger torque to overcome resistance. Furthermore, Figure 5 illustrates that in the low-speed region, a higher torque correlates with greater efficiency in the motor system. Consequently, utilizing a single rear motor drive is appropriate under no load conditions. However, when circling, the split force created by the articulated body suggests that using the front motor drive is preferable. Examining the data from Table A6, it becomes evident that under one-third of a load, the rear motor drive consumed less power and demonstrated higher system efficiency when moving forward. Conversely, when moving backward and circling, the front motor drive consumed less power and exhibited higher system efficiency. The data from Tables A7 and A8, representing the scenarios with two-thirds of a load and full load, respectively, indicate that the front motor drive predominantly consumed less power and displayed higher system efficiency.

Based on the above analysis, the following simple motor control rules are derived for transporting, as shown in Table 6. According to these rules and Equations (6) and (7), a comparison of the preferred controlled motor with the unselected motor at different speeds with no load revealed average power savings of 5.11%, 3.12%, and 6.88%. Additionally, the average improvement in motor system efficiency was 5.08%, 2.58%, and 0.95%, respectively, for forward, backward, and circling in a steady state. When at one-third of a load, the average power savings were 11.82%, 15.44%, and 0.34% with corresponding average improvements in motor system efficiency of 6.32%, 2.04%, and 1.43%. At two-thirds of a load, the average power savings were 40.91%, 33.65%, and 2.4%. When at a full load, the average power savings were 3.51%, 5.42%, and 4.74%. The results demonstrate that the DEWL can effectively reduce energy consumption by formulating a control method based on the variation of the vertical loads of the front and rear axle shafts.

$$\varepsilon = \frac{\sum_i \frac{\overline{P_{UI}}_{(unselected\ motor)} - \overline{P_{UI}}_{(preferred\ controlled\ motor)}}{\overline{P_{UI}}_{(preferred\ controlled\ motor)}}}{i} \tag{6}$$

$$\delta = \frac{\sum_i \overline{\eta_{sys}}_{(unselected\ motor)} - \overline{\eta_{sys}}_{(preferred\ controlled\ motor)}}{i} \tag{7}$$

ε is the percentage of average electrical power savings, $\overline{P_{UI}}_{(unselected\ motor)}$ is the average electrical power of the unselected motor, $\overline{P_{UI}}_{(preferred\ controlled\ motor)}$ is the average electrical power of the preferred controlled motor. δ represents the percentage increase in motor system efficiency, $\overline{\eta_{sys}}_{(unselected\ motor)}$ represents the average system efficiency of the unselected motor, and $\overline{\eta_{sys}}_{(preferred\ controlled\ motor)}$ represents the average system efficiency of the preferred controlled motor.

Table 6. Motor control rules of DEWL based on energy-saving in transporting condition.

Load	Forward	Backward	Circling
No	Rear motor	Rear motor	Front motor
1/3	Rear motor	Front motor	Front motor
2/3	Front motor	Front motor	Front motor
Full	Front motor	Front motor	Front motor

4.2. Control Scheme of Energy-Saving for DEWL under Pre-Shoveling Condition

According to Tables A9 and A10, the power reduction of the R1 condition over the F1 condition was 43.55% and 52.87%, and the system efficiency was improved by 21.23% and 23.05%. The power reduction of the R2 condition over the F2 condition was 43.91% and 43.61%, and the system efficiency was improved by 18.01% and 17.49%. The power reduction of the R1 condition over the D1 condition was 116.62% and 75.26%. The power reduction of the R2 condition over the D2 condition was 37.09% and 183.56%. The power reduction of the R3 condition over the D3 condition was 11.98% and 40.86%. Therefore, in pre-shoveling, utilizing a single rear motor drive effectively reduces electrical power consumption and improves the efficiency of the motor system. This is consistent with the energy-saving use of a single rear motor drive when traveling straight with no load. Such a configuration seamlessly aligns with the transition from the no-load transporting condition to the pre-shoveling condition, effectively circumventing any adverse impacts caused by motor switching.

4.3. Optimized Control Scheme for DEWL under Shoveling Condition

Indeed, addressing the issue of solving conditions requires careful consideration of cost-effectiveness and efficiency. One approach involves replacing the front axle motor with a higher torque motor. However, this option often incurs high costs. Alternatively, another viable solution involves adding a transmission between the front axle motor and the main reducer to increase the ratio. By doing so, the two motors can distribute different torque levels based on varying working conditions, enabling them to work in tandem and achieve optimal resource allocation. This approach offers a balance between effectiveness and affordability, making it a practical solution for improving loader performance.

Selecting a transmission that doubles the gear ratio is deemed sufficient for this application. This choice is based on the assumption that the front axle requires twice as much drive power when the load is fully concentrated in that axle. Therefore, doubling the gear ratio through the transmission adequately addresses the power requirements for optimal performance under such conditions. The selection of other parts remains unchanged from the existing setup. However, the addition of the transmission introduces a potential issue: the front axle motor may exceed its rated speed if the vehicle exceeds 0.5 times its maximum speed, rendering it inoperable. At this time, only the rear axle motor can work alone. Therefore, it is crucial to consider scenarios where the loader's speed exceeds half of its maximum speed and implement appropriate control measures. As the loader's center of gravity shifts towards the front wheel when the bucket is loaded with materials or during shoveling, the vertical load on the rear axle decreases, reducing its maximum static friction capacity. Taking into account factors such as loader bumps, we establish a critical value, denoted as *ß*, which represents the ratio between the real-time vertical load on the rear axle and the vertical load on the rear axle when carrying no load. This critical value helps determine the operational conditions for the loader. When this critical value exceeds or equals *ß*, indicating that the loader's center of gravity has not shifted significantly, both the front and rear axles can be normal to provide driving force. When the critical value falls below ß, indicating a shift in the loader's center of gravity, the rear axle motor can only supply torque equivalent to the product of this ratio and its rated torque. The remaining torque required is provided by the front axle motor. Therefore, it is necessary to consider a control method for the critical value case of the real-time vertical load of the rear axle and the vertical load of the rear axle when carrying no load. In summary, the analysis is considered in the following four scenarios:

1. When the speed of the loader exceeds half of its maximum speed, the front motor becomes inactive while the rear motor remains operational, providing the entirety of the required torque.
2. When the speed of the loader does not exceed half of its maximum speed, the front motor operates when the total demand torque is less than the rated torque of the front motor. The front motor provides the total demand torque, while the rear motor remains inactive.
3. When the following three conditions are met, the front motor becomes the primary drive while the rear motor acts as a support. The front motor delivers its rated torque, while the remaining torque is provided by the rear motor.
    a. Loader speed does not exceed half of its maximum speed.
    b. The total demand torque falls between the rated and maximum torque of the front motor.
    c. The ratio of the real-time vertical load on the rear axle to the unloaded rear axle's vertical load is equal to or greater than ß.
4. When conditions a and b mentioned in 3 are met, wihle conditon c is the opposite. The rear motor is the main work motor and the front motor is the auxiliary work motor. The demand torque of the rear motor is the maximum torque assigned to the motor before the rear wheels are lifted, and the front motor provides the remaining demand torque.

Therefore, the front and rear motor demand torque strategies of the new scheme are shown in Equations (8) and (9).

$$T_{F\_req} = \begin{cases} 0 & V_i > 0.5V_{\max} \\ \dfrac{T_{req}}{i_{org} \times i_{TX}} & V_i \leq 0.5V_{\max} \quad \& \quad \dfrac{T_{req}}{i_{org} \times i_{TX}} < T_{F\_rated} \\ T_{F\_rated} & V_i \leq 0.5V_{\max} \quad \& \quad T_{F\_rated} \leq \dfrac{T_{req}}{i_{org} \times i_{TX}} \leq T_{F\_\max} \quad \& \quad \dfrac{G_{Ri}}{G_R} \geq ß \\ \dfrac{T_{req}}{i_{org} \times i_{TX}} - T_{R\_req} & V_i \leq 0.5V_{\max} \quad \& \quad T_{F\_rated} \leq \dfrac{T_{req}}{i_{org} \times i_{TX}} \leq T_{F\_\max} \quad \& \quad \dfrac{G_{Ri}}{G_R} < ß \end{cases} \tag{8}$$

$$T_{R\_req} = \begin{cases} \dfrac{T_{req}}{i_{org} \times i_{TX}} & V_i > 0.5V_{\max} \\ 0 & V_i \leq 0.5V_{\max} \quad \& \quad \dfrac{T_{req}}{i_{org} \times i_{TX}} < T_{F\_rated} \\ \dfrac{T_{req}}{i_{org} \times i_{TX}} - T_{F\_req} & V_i \leq 0.5V_{\max} \quad \& \quad T_{F\_rated} \leq \dfrac{T_{req}}{i_{org} \times i_{TX}} \leq T_{F\_\max} \quad \& \quad \dfrac{G_{Ri}}{G_R} \geq ß \\ T_{F\_\max} \times \frac{G_{Ri}}{G_R} & V_i \leq 0.5V_{\max} \quad \& \quad T_{F\_rated} \leq \dfrac{T_{req}}{i_{org} \times i_{TX}} \leq T_{F\_\max} \quad \& \quad \dfrac{G_{Ri}}{G_R} < ß, \end{cases} \tag{9}$$

T_{req} is the total demand torque, T_{F_req} is the front motor demand torque, T_{R_req} is the rear motor demand torque, T_{F_rated} is the rated torque, $T_{F\_\max}$ is the maximum torque, i_{org} is the original total transmission ratio, i_{TX} is the ratio for the newly retrofitted transmission, V_i is the real-time speed of the loader, $V_{\max}$ is the maximum speed of the loader, G_{Ri} is the real-time vertical load on the rear axle, G_R is the rear axle vertical load at no load, and $ß$ is the critical value of the ratio between G_{Ri} and G_R.

5. Conclusions

This paper focuses on energy-saving-based torque distribution schemes for the DEWL during transporting, pre-shoveling, and shoveling. Through extensive testing across various scenarios, the operational rules of the DEWL are analyzed to devise an optimal control scheme for the current DEWL. At the same time, a new improvement method of the DEWL is proposed to address the shortcomings.

1. Under the same conditions, the torque and power consumption of an EWL with two motors without a mechanically connected drive shaft is better than an EWL with two motors with a mechanically connected drive shaft. Comparing a two-motor EWL without a mechanical connection to a two-motor EWL with a mechanical connection, the electric power consumption during single-motor forward driving exhibited average savings of 26.26%, 30.98%, 14.58% at one-third of a load, two-thirds of a load, and a full load. Similarly, during single-motor backward driving, the observed average savings were 40.40%, 34.88%, and 20.48% at the corresponding load levels. The EWL adopting a distributed solution is more energy-efficient.
2. The DEWL featuring no mechanical connection between the front and rear motors demonstrated significant electrical power savings during both forward and backward motion. When comparing single-front motor drive to dual-motor drive, there were electrical power savings of 38.10% during forward motion and 40.95% during backward motion. Similarly, comparing single-rear motor drive to dual-motor drive yielded savings of 39.58% during forward motion and 29.03% during backward motion. Consequently, the single-motor drive scheme emerges as the preferred option.
3. In the same situation, the mechanical power required to operate the front and rear motors individually shows little variation, yet there is a significant contrast in electric power consumption.
4. Under the transporting condition, the rear axle load surpasses the front axle load when the loader is carrying no load, and the energy-saving effect of adopting single front

motor drive is obvious. Comparing the preferred controlled motor and unselected motor at different speeds with no load, the average power savings were 5.11%, 3.12%, and 6.88%, respectively, for forward, backward, and circling in a steady state. At one-third of a load, the average power savings were 11.82%, 15.44%, and 0.34%. At two-thirds of a load, the average power savings were 40.91%, 33.65%, and 2.4%. At a full load, the average power savings were 3.51%, 5.42%, and 4.74%. Conversely, when the loader is loaded, the front axle load is greater than the rear axle load, and the energy-saving effect of using single rear motor drive is obvious. Under the pre-shoveling condition, notable energy savings were observed with a single rear motor drive.

5. When the DEWL was driven independently, the front motor shovel driving force was not enough and the rear wheels slipped easily. In order to solve this problem, an optimized control scheme with higher economy and lower transformation difficulty was proposed. The specific method is to add a transmission between the front axle motor and the main reducer to increase the total transmission ratio of the front axle. This modification makes it so that the maximum speed of the front wheel is half that of the rear wheel. The optimized control scheme is developed based on the change of DEWL dynamic parameters, combining the transporting and pre-shoveling energy-saving control schemes. A new distributed electric wheel loader [1] conforming to Equations (8) and (9) has been developed. The prototype is undergoing adjustments to certain mechanical structures and testing of subsystems. The actual application of Equations (8) and (9) will take place soon.

Author Contributions: Conceptualization, W.S. and C.J.; funding acquisition, W.S.; investigation, Y.H.; methodology, W.S. and Y.H.; resources, Y.H. and X.F.; software, W.S.; supervision, C.J.; validation, W.S.; writing—original draft, W.S. and X.F. All authors have read and agreed to the published version of the manuscript.

Funding: This research was funded by the Sudian Yingcai Engineering Project from the Jiangsu Vocational College of Electronics and Information, the Huai'an City Science and Technology project (Grant No. HABL202127), Huai'an City Science and Technology project (Grant No. HABZ202319), and Huai'an New Energy Vehicle Technology Public Service Platform (Grant No. HAP202313).

Data Availability Statement: The original contributions presented in the study are included in the article, further inquiries can be directed to the corresponding author.

Conflicts of Interest: The authors declare no conflicts of interest.

Appendix A

The explanation of Status in the table is shown in Table 3, where subscripts 1–3 represent the three-test data, and all the results are the average of the three measurements. $\overline{n}$ represents the average speed of the driving motor. $\overline{T}$ represents the average torque of the driving motor. $\overline{P_T}$ and $\overline{P_{UI}}$ represents the average mechanical power and electrical power of the driving motor. $\overline{\eta_{sys}}$ represents the average system efficiency of the driving motor. The system efficiency is equivalent to the ratio of the controller efficiency to the motor efficiency and is also equal to the ratio of the mechanical power to the electric power.

Table A1. Data calculated in transporting condition under 1/3 load (Front and rear motor with mechanical connection by single-motor drive).

Status	$\overline{n}$ (rpm)	$\overline{T}$ (N·m)	$\overline{P_T}$ (kW)	$\overline{P_{UI}}$ (kW)	$\overline{\eta_{sys}}$ (%)
$FF_{1\text{-}3}$	199.51	98.9	2.06	4.06	50.74
	399.48	115.74	4.83	7.87	61.37
	599.54	119.3	7.49	8.92	83.97
	799.52	125.87	10.53	16.26	64.76
	999.55	130.01	13.6	19.66	69.18

Table A1. *Cont.*

Status	$\overline{n}$ (rpm)	$\overline{T}$ (N·m)	$\overline{P_T}$ (kW)	$\overline{P_{UI}}$ (kW)	$\overline{\eta_{sys}}$ (%)
$FB_{1\text{-}3}$	−200.49	−125.36	2.63	4.84	54.34
	−400.48	−129.28	5.42	8.27	65.54
	−600.61	−132.89	8.35	14.27	58.51
	−800.55	−135.29	11.33	16.83	67.32
	−1000.42	−139.69	14.62	20.56	71.11
$FC_{1\text{-}3}$	199.49	116.79	2.44	5.55	43.96
	399.46	132.44	5.54	9.4	58.94
	599.58	153.39	9.62	15.34	62.71
	798.9	176.93	14.79	21.71	68.13
$RF_{1\text{-}3}$	−200.48	−111.69	2.34	3.76	62.23
	−400.5	−112.67	4.72	6.77	69.72
	−600.43	−124.66	7.83	12.83	61.03
	−800.47	−125.07	10.48	16.01	65.46
	−1000.39	−129.99	13.61	19.48	69.87
$RB_{1\text{-}3}$	199.51	114.34	2.39	4.79	49.90
	399.56	121.74	5.09	7.36	69.16
	599.59	126.95	7.97	15.38	51.82
	799.53	134.05	11.22	17.3	64.86
	999.56	136.17	14.24	20.31	70.11
$RC_{1\text{-}3}$	−200.54	−124.67	2.61	5.55	47.03
	−400.48	−136.96	5.74	9.65	59.48
	−600.52	−151.94	9.55	15.19	62.87
	−799.91	−175.93	14.72	22.41	65.68

Table A2. Data calculated in transporting condition under 2/3 load (Front and rear motor with mechanical connection by single-motor drive).

Status	$\overline{n}$ (rpm)	$\overline{T}$ (N·m)	$\overline{P_T}$ (kW)	$\overline{P_{UI}}$ (kW)	$\overline{\eta_{sys}}$ (%)
$FF_{1\text{-}3}$	199.38	124.64	2.60	4.70	55.32
	399.66	134.29	5.62	9.27	60.63
	594.63	139.29	8.66	15.10	57.35
	798.11	146.59	12.24	17.16	71.33
	1004.64	139.98	14.70	21.38	68.76
$FB_{1\text{-}3}$	−200.25	−143.31	3.00	5.40	55.56
	−400.35	−145.78	6.10	10.19	59.86
	−610.00	−155.34	9.94	19.71	50.43
	−812.03	−154.31	13.13	20.88	62.88
$FC_{1\text{-}3}$	199.50	180.85	3.77	6.93	54.40
	399.70	191.78	8.02	12.43	64.52
	599.71	204.50	12.83	19.62	65.39
	799.61	225.60	18.85	28.60	65.91
$RF_{1\text{-}3}$	−200.7	−120.12	2.52	4.55	55.38
	−402.79	−124.12	5.21	7.65	68.10
	−597.82	−142.57	8.92	15.17	58.80
	−799.51	−152.51	12.76	22.25	57.35
	−999.29	−147.71	15.45	25.94	59.56
$RB_{1\text{-}3}$	199.47	130.4	2.72	5.94	45.79
	400.36	139.62	5.85	10.31	56.74
	597.94	162.52	10.17	15.7	64.78
	802.86	157.09	13.2	18.1	72.93
	1001.76	166.04	17.4	26.36	66.01
$RC_{1\text{-}3}$	−200.51	−140.19	2.94	6.33	46.45
	−400.57	−149.71	6.27	10.68	58.71
	−600.52	−172.89	10.86	17.28	62.85
	−800.1	−199.5	16.7	25.44	65.64

Table A3. Data calculated in transporting condition under full load (Front and rear motor with mechanical connection by single-motor drive).

Status	$\overline{n}$ (rpm)	$\overline{T}$ (N·m)	$\overline{P_T}$ (kW)	$\overline{P_{UI}}$ (kW)	$\overline{\eta_{sys}}$ (%)
$FF_{1\text{-}3}$	199.48	154.92	3.23	6.14	52.61
	399.5	164.9	6.89	10.35	66.57
	599.62	169.59	10.64	17.03	62.48
	799.63	179.77	15.05	22.64	66.48
	999.65	184.5	19.29	26.75	72.11
$FB_{1\text{-}3}$	−200.53	−177.85	3.73	5.91	63.11
	−400.61	−177.7	7.45	10.88	68.47
	−600.5	−185.33	11.65	17.38	67.03
	−800.69	−185.71	15.56	23.06	67.48
	−1000.39	−201.19	21.05	29.02	72.54
$FC_{1\text{-}3}$	199.46	180.85	3.77	6.93	54.40
	399.49	191.78	8.02	12.43	64.52
	599.63	204.5	12.83	19.62	65.39
	799.18	225.6	18.85	28.6	65.91
$RF_{1\text{-}3}$	−200.45	−157.36	3.3	5.24	62.98
	−400.53	−165.95	6.96	10.84	64.21
	−600.51	−170.85	10.74	14.87	72.23
	−800.65	−178	14.92	20.6	72.43
$RB_{1\text{-}3}$	199.45	176.82	3.69	6.49	56.86
	399.48	177.48	7.42	10.79	68.77
	599.35	181.86	11.41	15.28	74.67
	799.43	187.8	15.72	19.93	78.88
$RC_{1\text{-}3}$	−200.45	−177.46	3.72	7.06	52.70
	−400.51	−190.41	7.98	12.32	52.69
	−600.46	−198.64	12.48	18.78	64.77
	−800.37	−220.27	18.43	26.51	66.45

Table A4. Data calculated in transporting condition under no load (Front and rear motor without mechanical connection by dual-motor drive).

Status	$\overline{n}$ (rpm)		$\overline{T}$ (N·m)		$\overline{P_T}$ (kW)		$\overline{P_{UI}}$ (kW)		$\overline{\eta_{sys}}$ (%)	
$DF_{1\text{-}3}$	199.44	−200.51	−120.45	−236.81	−2.52	4.97	−5.21	10.03	48.25	49.56
	399.27	−400.73	−135.08	−253.53	−5.65	10.64	−9.19	17.05	61.50	62.40
	599.74	−600.44	−122.63	−247.61	−7.71	15.56	−22.75	34.27	33.88	45.42
	799.19	−800.75	−140.69	−269.29	−11.78	22.57	−31.08	45.73	37.91	49.37
	999.78	−1000.38	−126.00	−261.17	−13.20	27.36	−23.72	42.15	55.64	64.91
$DB_{1\text{-}3}$	−200.55	199.41	162.82	282.28	−3.42	5.89	−8.44	13.35	40.52	44.11
	−400.27	399.63	193.92	311.43	−8.13	13.03	−14.54	22.60	55.91	57.66
	−600.46	599.64	176.75	302.83	−11.12	19.01	−20.91	33.28	53.18	57.12
	−800.47	799.24	180.15	309.36	−15.11	25.88	−41.19	55.77	36.68	46.41
	−1000.70	999.60	176.74	314.37	−18.53	32.89	−34.92	53.65	53.06	61.31
$DC_{1\text{-}3}$	199.45	−200.52	−119.70	−235.38	−2.50	4.94	−5.23	11.03	47.80	44.79
	399.27	−400.73	−135.08	−253.53	−5.65	10.64	−9.19	18.05	61.48	58.95
	599.74	−600.44	−122.63	−247.61	−7.70	15.57	−22.75	35.27	33.85	44.15
	799.19	−800.75	−140.69	−269.29	−11.78	22.58	−31.08	46.73	37.90	48.32
	999.78	−1000.38	−126.00	−261.17	−13.19	27.36	−23.72	43.15	55.61	63.41

Table A5. Data calculated in transporting condition under no load (Front and rear motor without mechanical connection by single-motor drive).

Status	$\overline{n}$ (rpm)	$\overline{T}$ (N·m)	$\overline{P_T}$ (kW)	$\overline{P_{UI}}$ (kW)	$\overline{\eta_{sys}}$ (%)
$FF_{1\text{-}3}$	199.52	74.30	1.55	2.91	53.26
	399.52	82.55	3.45	4.64	74.35
	599.68	88.85	5.58	6.37	87.60
	799.67	93.01	7.79	9.57	81.40
	999.40	97.04	10.16	12.80	79.38
$FB_{1\text{-}3}$	−199.49	−78.06	1.63	2.90	56.21
	−400.42	−85.60	3.59	5.53	64.92
	−600.50	−87.17	5.48	6.86	79.88
	−800.39	−98.70	8.27	9.78	84.56
	−1000.50	−100.24	10.50	13.13	79.97
$FC_{1\text{-}3}$	199.59	101.70	2.13	4.94	43.12
	399.54	121.80	5.10	7.68	66.41
	599.86	139.99	8.79	13.88	63.33
	799.69	162.66	13.62	18.47	73.74
$RF_{1\text{-}3}$	−200.48	−78.33	1.64	2.82	58.16
	−400.51	−81.94	3.44	4.55	75.60
	−600.41	−86.17	5.41	5.68	95.25
	−800.50	−94.93	7.95	8.92	89.13
	−1000.33	−100.91	10.56	12.68	83.28
$RB_{1\text{-}3}$	199.48	80.89	1.69	2.89	58.48
	399.51	85.16	3.56	5.51	64.61
	599.56	91.22	5.72	6.50	88.00
	799.55	94.16	7.87	9.07	86.77
	999.30	99.65	10.42	12.93	80.59
$RC_{1\text{-}3}$	−200.52	−109.71	2.30	5.12	44.92
	−400.56	−131.91	5.53	9.27	59.65
	−600.42	−150.73	9.48	14.29	66.34
	−800.40	−156.64	13.13	18.51	70.93

Table A6. Data calculated in transporting condition under 1/3 load (Front and rear motor without mechanical connection by single-motor drive).

Status	$\overline{n}$ (rpm)	$\overline{T}$ (N·m)	$\overline{P_T}$ (kW)	$\overline{P_{UI}}$ (kW)	$\overline{\eta_{sys}}$ (%)
$FF_{1\text{-}3}$	199.61	87.67	1.83	3.79	48.28
	399.44	97.20	4.07	6.81	59.77
	599.50	102.14	6.41	8.22	77.98
	799.48	111.59	9.34	11.96	78.09
	999.60	122.58	12.83	16.04	79.99
$FB_{1\text{-}3}$	−200.39	−96.80	1.93	3.31	58.31
	−400.52	−100.10	4.20	6.37	65.93
	−600.54	−106.37	6.69	8.05	83.11
	−800.48	−110.79	9.29	11.28	82.36
	−1000.38	−115.56	12.11	14.88	81.38
$FC_{1\text{-}3}$	199.42	134.66	2.81	5.55	50.63
	399.42	140.51	5.88	9.72	60.49
	599.40	162.02	10.17	16.30	62.39
	799.49	176.76	14.80	22.63	65.40

Table A6. *Cont.*

Status	$\overline{n}$ (rpm)	$\overline{T}$ (N·m)	$\overline{P_T}$ (kW)	$\overline{P_{UI}}$ (kW)	$\overline{\eta_{sys}}$ (%)
$RF_{1\text{-}3}$	−201.04	−84.13	1.77	3.02	58.61
	−400.50	−97.32	4.08	5.70	71.58
	−600.52	−111.80	7.03	8.89	79.08
	−800.58	−104.32	8.75	10.36	84.46
	−1000.54	−117.96	12.36	15.10	81.85
$RB_{1\text{-}3}$	199.38	104.42	2.18	4.19	52.03
	399.40	103.04	4.30	6.63	64.86
	599.47	103.38	6.48	9.39	69.01
	799.51	117.48	9.83	13.15	74.75
	999.46	120.92	12.65	16.86	75.03
$RC_{1\text{-}3}$	−200.58	−130.44	2.74	5.56	49.28
	−400.56	−139.94	5.87	9.79	59.96
	−600.51	−162.70	10.23	15.45	66.21
	−800.20	−196.50	16.46	23.30	70.64

Table A7. Data calculated in transporting condition under 2/3 load (Front and rear motor without mechanical connection by single-motor drive).

Status	$\overline{n}$ (rpm)	$\overline{T}$ (N·m)	$\overline{P_T}$ (kW)	$\overline{P_{UI}}$ (kW)	$\overline{\eta_{sys}}$ (%)
$FF_{1\text{-}3}$	200.18	106.10	2.22	3.77	58.89
	396.46	112.69	4.68	6.88	68.02
	596.53	116.02	7.25	9.11	79.58
	806.51	129.64	10.95	11.46	95.55
	995.83	128.65	13.42	13.92	96.41
$FB_{1\text{-}3}$	−202.40	−110.68	2.35	4.91	47.86
	−400.45	−102.69	4.31	6.90	62.46
	−607.24	−108.13	6.86	10.19	67.32
	−817.12	−101.23	8.66	11.49	75.37
	−1020.25	−124.60	13.31	17.52	75.97
$FC_{1\text{-}3}$	199.50	141.58	2.96	6.52	45.40
	399.49	140.53	5.88	9.93	59.21
	599.58	179.20	11.25	17.70	63.56
	800.05	219.67	18.41	24.83	74.14
$RF_{1\text{-}3}$	−202.32	−126.71	2.68	4.71	56.90
	−396.74	−129.21	5.37	7.90	67.97
	−604.28	−136.96	8.67	14.20	61.06
	−790.05	−131.68	10.89	14.83	73.43
	−997.89	−136.19	14.23	24.99	56.94
$RB_{1\text{-}3}$	199.36	109.97	2.30	5.27	43.64
	397.29	115.79	4.82	9.23	52.22
	598.30	122.78	7.69	13.91	55.28
	806.82	141.71	11.97	16.61	72.07
	1000.47	161.47	16.92	25.59	66.12
$RC_{1\text{-}3}$	−200.44	−144.02	3.02	5.98	50.50
	−400.49	−160.11	6.71	10.64	63.06
	−600.77	−170.14	10.70	16.47	64.97
	−800.74	−202.01	16.94	24.89	68.06

Table A8. Data calculated in transporting condition under full load (Front and rear motor without mechanical connection by single-motor drive).

Status	$\overline{n}$ (rpm)	$\overline{T}$ (N·m)	$\overline{P_T}$ (kW)	$\overline{P_{UI}}$ (kW)	$\overline{\eta_{sys}}$ (%)
$FF_{1\text{-}3}$	199.43	128.59	2.69	5.48	49.09
	399.86	140.14	5.87	9.45	62.12
	599.37	155.13	9.74	12.84	75.86
	798.72	167.49	14.01	19.02	73.66
	999.08	160.49	16.79	22.46	74.76
$FB_{1\text{-}3}$	−200.32	−144.20	3.03	5.89	51.44
	−400.18	−151.05	6.33	9.63	65.73
	−599.80	−160.21	10.06	11.29	89.11
	−800.72	−154.08	12.92	16.21	79.70
	−1000.22	−165.89	17.38	22.63	76.80
$FC_{1\text{-}3}$	199.53	175.16	3.66	8.056	45.43
	399.52	185.58	7.76	13.87	55.95
	599.81	209.37	13.15	22.19	59.26
	799.18	238.62	19.97	31.34	63.72
$RF_{1\text{-}3}$	−200.40	−138.79	2.91	5.09	57.17
	−400.58	−146.02	6.13	9.81	62.49
	−600.50	−150.94	9.49	11.20	84.73
	−800.71	−166.25	13.94	19.05	73.18
	−1000.73	−165.13	17.31	22.67	76.36
$RB_{1\text{-}3}$	199.79	144.72	3.03	5.72	52.97
	398.90	156.04	6.52	9.84	66.26
	599.62	155.80	9.78	11.99	81.57
	800.08	159.63	13.37	19.32	69.20
	999.88	166.63	17.45	23.18	75.28
$RC_{1\text{-}3}$	−200.45	−175.97	3.69	7.31	50.48
	−400.59	−195.45	8.20	13.27	61.79
	−600.84	−214.85	13.52	21.14	63.95
	−800.77	−247.34	20.74	31.57	65.70

Table A9. Data calculated in pre-shoveling condition (Front and rear motor without mechanical connection by single-motor drive).

Status	Direction	$\overline{T}$ (N·m)	$\overline{P_T}$ (kW)	$\overline{P_{UI}}$ (kW)	$\overline{\eta_{sys}}$ (%)
$F1_{1\text{-}3}$	Forward	295.93	18.58	42.49	43.73
	Backward	−279.32	17.56	38.92	45.12
$F2_{1\text{-}3}$	Forward	417.50	26.18	64.83	40.39
	Backward	−366.72	23.02	55.03	41.84
$R1_{1\text{-}3}$	Forward	−305.74	19.20	29.60	64.96
	Backward	276.47	17.35	25.46	68.17
$R2_{1\text{-}3}$	Forward	−418.95	26.30	45.05	58.40
	Backward	362.31	22.73	38.32	59.33
$R3_{1\text{-}3}$	Forward	−537.36	33.75	60.28	56.03
	Backward	501.76	31.47	56.70	55.50
$R4_{1\text{-}3}$	Forward	−605.76	38.08	71.90	52.99
	Backward	605.83	38.00	71.34	53.31

Table A10. Data calculated in pre-shoveling condition (Front and rear motor without mechanical connection by dual-motor drive).

Status	Direction	$\overline{T}$ (N·m)		$\overline{P_T}$ (kW)		$\overline{P_{UI}}$ (kW)		$\overline{\eta_{sys}}$	
$D1_{1\text{-}3}$	Forward	259.29	−167.30	16.26	10.52	42.02	22.10	38.70	47.60
	Backward	−156.93	213.27	9.87	13.38	21.70	22.92	45.49	58.37
$D2_{1\text{-}3}$	Forward	259.65	−234.18	16.30	14.71	36.65	25.11	44.47	58.58
	Backward	−266.54	184.31	16.75	44.21	37.89	70.77	44.21	62.47
$D3_{1\text{-}3}$	Forward	106.85	−470.85	6.65	29.39	20.96	46.54	31.73	63.15
	Backward	−209.68	306.19	13.17	34.13	38.59	41.28	34.13	82.67

References

1. Culpin, C. *Farm Machinery*; Read Books Ltd.: Redditch, UK, 2013; ISBN 1446547787.
2. Bavendiek, I.R.; Kremmer, M.; Pfab, I.H. Selected Machine Examples. In *Mobile Working Machines*; SAE: Warrendale, PA, USA, 2020; p. 323.
3. Mocera, F.; Somà, A. A Review of Hybrid Electric Architectures in Construction, Handling and Agriculture Machines. In *New Perspectives on Electric Vehicles*; IntechOpen: London, UK, 2021.
4. Paraszczak, J.; Svedlund, E.; Fytas, K.; Laflamme, M. Electrification of loaders and trucks–a step towards more sustainable underground mining. *Renew. Energy Power Qual. J.* **2014**, *12*, 81–86. [CrossRef]
5. Huang, P.; Xu, L.; Luo, C.; Zhang, J.; Chi, F.; Zhang, Q.; Zhou, J. A study on noise reduction of gear pumps of wheel loaders based on the ICA model. *Int. J. Environ. Res. Public Health* **2019**, *16*, 999. [CrossRef] [PubMed]
6. De Almeida, C.M.; de Castro Neves, T.; Arroyo, C.; Campos, P. Truck-and-Loader versus Conveyor Belt System: An Environmental and Economic Comparison. In Proceedings of the 27th International Symposium on Mine Planning and Equipment Selection-MPES 2018; Springer International Publishing: New York, NY, USA, 2019; pp. 307–318.
7. Zhang, Q.; Wang, F.; Cheng, M.; Xu, B. Energy efficiency improvement of battery powered wheel loader with an electric-hydrostatic hybrid powertrain. *Proc. Inst. Mech. Eng. Part D J. Automob. Eng.* **2023**, *237*, 75–88. [CrossRef]
8. Available online: https://www.ccm-1.com/news/4715.html (accessed on 17 February 2024).
9. Available online: https://zj.lmjx.net/zhuangzaiji/diandong/ (accessed on 17 February 2024).
10. Yang, Z.; Liu, S.; Wan, Y.; Han, Y. *Generation Mechanism Analysis and Calculation Method of Loader Parasitic Power Based on Tire Radius Difference*; SAE Technical Paper; SAE International: Warrendale, PA, USA, 2022. [CrossRef]
11. Shuang, L. *Calculation Method and Experimental Study of Parasitic Power of Wheel Loader*; Jilin University: Changchun, China, 2022.
12. Jiang, T.; Geng, C.; Xue, Q.; Zhang, X. Torque distribution strategy of FRID EV based on energy consumption optimization. *J. Beijing Jiaotong Univ.* **2019**, *43*, 102–109. [CrossRef]
13. Yang, Z.; Wang, J.; Gao, G.; Shi, X. Research on Optimized Torque-Distribution Control Method for Front/Rear Axle Electric Wheel Loader. *Math. Probl. Eng.* **2017**, *2017*, 7076583. [CrossRef]
14. Fei, X.; Han, Y.; Wong, S.V.; Azman, M.A. Efficiency Comparison of Electric Wheel Loader Powertrains with Dual Motor Input in Distributed Driving Modes. *World Electr. Veh. J.* **2023**, *14*, 298. [CrossRef]
15. Cai, S.; Chen, Q.; Lin, T.; Xu, M.; Ren, H. Automatic Shift Control of an Electric Motor Direct Drive for an Electric Loader. *Machines* **2022**, *10*, 403. [CrossRef]
16. Uebel, K.; Raduenz, H.; Krus, P.; De Negri, V.J. Design optimisation strategies for a hydraulic hybrid wheel loader. In Proceedings of the BATH/ASME 2018 Symposium on Fluid Power and Motion Control, Bath, UK, 12–14 September 2018.
17. Oh, K.; Kim, H.; Ko, K.; Kim, P.; Yi, K. Integrated wheel loader simulation model for improving performance and energy flow. *Autom. Constr.* **2015**, *58*, 129–143. [CrossRef]
18. Gao, G.; Wang, J.; Ma, T.; Han, Y.; Yang, X.; Li, X. Optimisation strategy of torque distribution for the distributed drive electric wheel loader based on the estimated shovelling load. *Veh. Syst. Dyn.* **2022**, *60*, 2036–2054. [CrossRef]
19. Sondkar, P.; Gharpure, S.; Schrand, V.; Attibele, P. Longitudinal vehicle dynamics modeling for AWD/4WD vehicles to study torque split between front and rear axles. *SAE Int. J. Adv. Curr. Pract. Mobil.* **2020**, *2*, 2987–2996. [CrossRef]
20. Yuan, X.; Wang, J. Torque distribution strategy for a front-and rear-wheel-driven electric vehicle. *IEEE Trans. Veh. Technol.* **2012**, *61*, 3365–3374. [CrossRef]
21. Shuaipeng, Q.; Minghui, H.; Kaibin, C.; Chunyun, F. Optimal driving force distribution strategy for multi-axle electric vehicles. *J. Chongqing Univ. (Nat. Sci. Ed.)* **2021**, *44*, 31–42. [CrossRef]
22. Wang, W.; Li, J.; Li, X.; Li, Z.; Guo, N. Multi-Objective Collaborative Control Method for Multi-Axle Distributed Vehicle Assisted Driving. *Appl. Sci.* **2023**, *13*, 7769. [CrossRef]
23. Jin, L.; Tian, D.; Zhang, Q.; Wang, J. Optimal Torque Distribution Control of Multi-Axle Electric Vehicles with In-wheel Motors Based on DDPG Algorithm. *Energies* **2020**, *13*, 1331. [CrossRef]
24. Qiu, L.; Zhu, S.; Liu, D.; Xiang, Z.; Fu, H.; Chen, H. Research on the Torque Control Strategy of a Distributed 4WD Electric Vehicle Based on Economy and Stability Control. *Electronics* **2022**, *11*, 3546. [CrossRef]

25. Liu, M.; Xu, L.; Zhou, Z. Design of a Load Torque Based Control Strategy for Improving Electric Tractor Motor Energy Conversion Efficiency. *Math. Probl. Eng.* **2016**, *2016*, 2548967. [CrossRef]
26. Zhang, S.; Wen, C.; Ren, W.; Luo, Z.; Xie, B.; Zhu, Z.; Chen, Z. A joint control method considering travel speed and slip for reducing energy consumption of rear wheel independent drive electric tractor in ploughing. *Energy* **2023**, *263*, 126008. [CrossRef]
27. Fei, X.; Han, Y.; Wong, S.V. An Overview of and Prospects for Research on Energy Savings in Wheel Loaders. *Automot. Exp.* **2023**, *6*, 133–148. [CrossRef]
28. Li, X.; Duan, C.; Bai, K.; Yao, Z. Operating Performance of Pure Electric Loaders with Different Types of Motors Based on Simulation Analysis. *Energies* **2021**, *14*, 617. [CrossRef]
29. Cao, B.; Liu, C.; Chen, W.; Tan, P.; Yang, J. Shovel-loading cooperative control of loader under typical working conditions. *ISA Trans.* **2023**, *142*, 702–715. [CrossRef]
30. Fei, X.; Han, Y.; Wong, S.V.; Azman, M.A.; Shen, W. Design and Testing of Innovative Type of Dual-Motor Drive Electric Wheel Loader. *Energies* **2024**, *17*, 1542. [CrossRef]